

DNA damage-induced cell death relies on SLFN11-dependent cleavage of distinct type II tRNAs

Manqing Li^{1,4*}, Elaine Kao^{1,4}, Dane Malone^{1,4}, Xia Gao¹, Jean Y.J. Wang^{1,2,3} and Michael David^{1,2,*}

Transcriptome analysis reveals a strong positive correlation between human Schlafen family member 11 (SLFN11) expression and the sensitivity of tumor cells to DNA-damaging agents (DDAs). Here, we show that SLFN11 preferentially inhibits translation of the serine/threonine kinases ATR and ATM upon DDA treatment based on distinct codon usage without disrupting early DNA damage response signaling. Type II transfer RNAs (tRNAs), which include all serine and leucine tRNAs, are cleaved in a SLFN11-dependent manner in response to DDAs. Messenger RNAs encoded by genes with high TTA (Leu) codon usage, such as ATR, display utmost susceptibility to translational suppression by SLFN11. Specific attenuation of tRNA-Leu-TAA sufficed to ablate ATR protein expression and restore the DDA sensitivity of SLFN11-deficient cells. Our study uncovered a novel mechanism of codon-specific translational inhibition via SLFN11-dependent tRNA cleavage in the DNA damage response and supports the notion that SLFN11-deficient tumor cells can be resensitized to DDAs by targeting ATR or tRNA-Leu-TAA.

DNA-damaging agents (DDAs) represent the largest group of cancer drugs; however, primary or secondary resistance severely limits their effectiveness. Two large-scale transcriptome analyses in cancer cells revealed that human Schlafen family member 11 (SLFN11)—a protein we previously found to inhibit translation of human immunodeficiency virus (HIV) proteins due to atypical codon usage in the viral RNA¹—sensitizes cancer cells to DDAs^{2,3}. SLFN11 belongs to the gene family of *Schlafen* (*SLFN*), which are exclusively found in mammals with the notable exception of orthopoxviruses⁴. *SLFNs* share no significant homology with other proteins beyond an N-terminal divergent AAA (ATPases associated with various cellular activities) domain, and in the case of the longer family members such as SLFN11, a putative C-terminal DNA/RNA helicase domain⁵. Based on our knowledge gained from the study of SLFN11 in HIV protein synthesis, we hypothesized that SLFN11 may sensitize cells to DNA damage by inhibiting the synthesis of proteins vital to survival after DNA damage if the corresponding genes also harbor deviant codon usage. To this end, we calculated the codon adaptation index (CAI) of genes involved in DNA damage response signaling and multiple DNA damage repair mechanisms, including homology-directed repair (HDR), nonhomologous end joining (NHEJ), DNA mismatch repair (MMR), nucleotide excision repair (NER) and base excision repair (BER), using 80 highly expressed ribosomal proteins as a reference gene set^{6–9}. Contrasting the very high average CAI (0.79) of the most abundantly expressed cellular proteins¹⁰, the DNA damage response signaling-related genes displayed an average CAI as low as 0.66, comparable to the average CAI (0.60) of HIV-1 genes (Supplementary Table 1). Importantly, the two components central to the DNA damage response, protein serine/threonine kinases ATR and ATM^{11,12}, presented CAIs as low as 0.65 for ATR and 0.64 for ATM, in striking contrast to the highly expressed glyceraldehyde-3-phosphate dehydrogenase (GAPDH) with a CAI of 0.81. Considering the additional impact of the long coding sequences of ATR (2,644 amino acids) and ATM (3,056 amino acids), it appears that the translation of both ATR and ATM may indeed be a

probable target for SLFN11. Interestingly, we noted that genes involved in HDR, NHEJ and MMR also display lower average CAIs (0.67, 0.69 and 0.69, respectively) than genes affiliated with NER and BER (0.73 and 0.74) (Supplementary Tables 2 and 3).

Results

To investigate the potential posttranscriptional control of ATR and ATM expression by SLFN11, we generated stable polyclonal derivatives from the pancreatic cancer cell line COLO 357/FG (hereafter referred to as FG cells)¹³ and human embryonic kidney cells 293 (HEK 293) cells (hereafter referred to as 293 cells) using two independent lentivirus-based short hairpin RNA (shRNA) constructs against SLFN11 to permanently silence SLFN11 expression. Crucially, silencing SLFN11 expression conferred significant resistance of both FG and 293 cells to the topoisomerase I inhibitor camptothecin (CPT) (Fig. 1a,d), as well as other DDAs, including the topoisomerase II inhibitor mitoxantrone, the nucleoside analog gemcitabine and the DNA-alkylating and cross-linking agent chlorambucil (Fig. 1g–i). Further, microscopic imaging of live cell cultures confirmed that CPT treatment induced cell death in SLFN11-expressing cells but not in SLFN11-deficient cells (Fig. 1j).

To determine whether SLFN11 affects translation of ATR and ATM in response to DNA damage, we first analyzed the expression levels of both ATR and ATM after CPT treatment. Indeed, expression of both proteins was significantly downregulated after 24 or 48 h of CPT exposure in FG and 293 cells, but were barely affected in their SLFN11-lacking matched counterparts (Fig. 1b,e). In contrast, both ATR and ATM messenger RNA (mRNA) levels stayed constant or were upregulated on CPT treatment (Fig. 1c,f). To determine whether the elevated expression of ATR or ATM proteins in SLFN11-deficient cells on CPT treatment is essential for their resistance to DDAs, we abolished the expression of ATR or ATM with corresponding small interfering RNAs (siRNAs) in both parental and SLFN11-deficient FG and 293 cells (Fig. 2a,c). Attenuation of ATR expression completely restored the sensitivity of SLFN11-deficient cell lines to CPT treatment, whereas silencing of

¹Section of Molecular Biology, Division of Biological Sciences, University of California, San Diego, La Jolla, CA, USA. ²Moores Cancer Center, University of California, San Diego, La Jolla, CA, USA. ³Division of Hematology-Oncology, Department of Medicine, University of California, San Diego, La Jolla, CA, USA. ⁴These authors contributed equally: Manqing Li, Elaine Kao, and Dane Malone. *e-mail: m5li@ucsd.edu; midavid@ucsd.edu

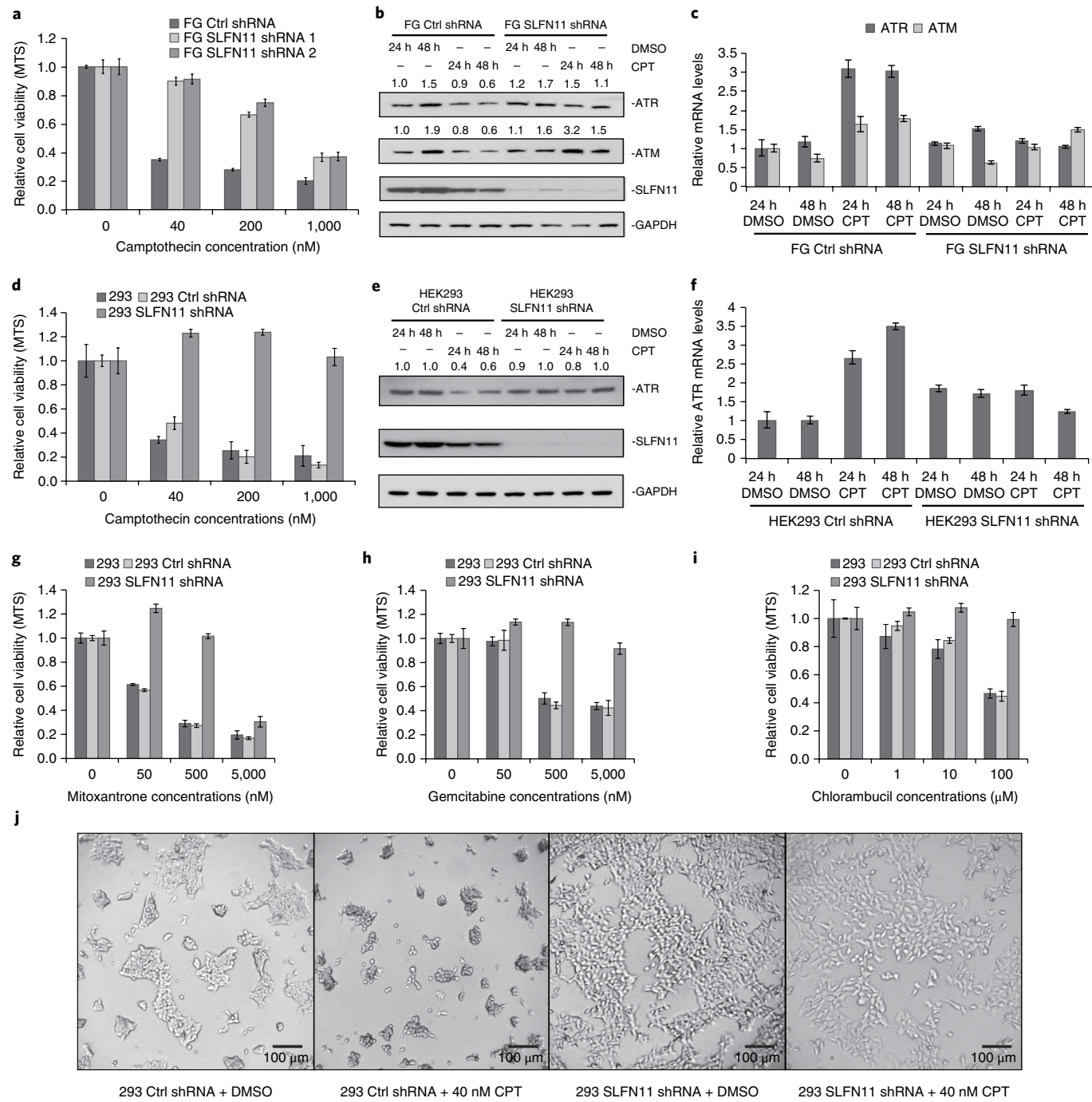


Fig. 1 | SLFN11 selectively inhibits ATR/ATM protein expression and sensitizes cells to death on treatment with DDAs. **a**, The relative viability of FG cells expressing control (Ctrl) or SLFN11 shRNA was measured by MTS assay after 48 h of CPT or DMSO treatment (error bars indicate mean \pm s.d., $n=3$ independent cell cultures). **b**, Immunoblot analysis of ATR and ATM protein levels after 40 nM CPT or DMSO treatment in FG cells expressing control or SLFN11 shRNA. **c**, Relative ATR and ATM mRNA levels as determined by qPCR in FG cells expressing Ctrl or SLFN11 shRNA after 40 nM CPT or DMSO treatment (mean \pm s.d., $n=3$ independent cell cultures). **d–f**, As in **a–c**, except with HEK 293 cells. **g–i**, As in **d** with additional DDAs as specified. **j**, Microscopic images of HEK 293 cell cultures after 24 h of CPT. Uncropped images are shown in Supplementary Dataset 1.

ATM expression failed to do so (Fig. 2b,d). The inherently SLFN11-deficient pancreatic tumor cell line, MIA PaCa-2, was also sensitized to CPT treatment by siRNA-mediated suppression of ATM expression, corroborating these observations (Fig. 2e–g). Inhibition of ATR kinase activity by the small-molecule ATR inhibitor VE-822 also sensitized SLFN11-deficient cells to CPT treatment in a dose-dependent manner (Fig. 2h–k). Our data also suggest that expression

of SLFN11 did not affect the early DNA damage response signaling, as reflected by phosphorylation of checkpoint kinase 1 (CHK1) at serine 317 by ATR (Fig. 2i, lanes 1, 2, 6, 7).

We performed ^{35}S methionine and ^{35}S cysteine labeling and pulse-chase experiments to determine the synthesis rate and stability of ATR protein on CPT treatment. As anticipated, in the presence of SLFN11, ATR protein synthesis was nearly abolished after 24 h of

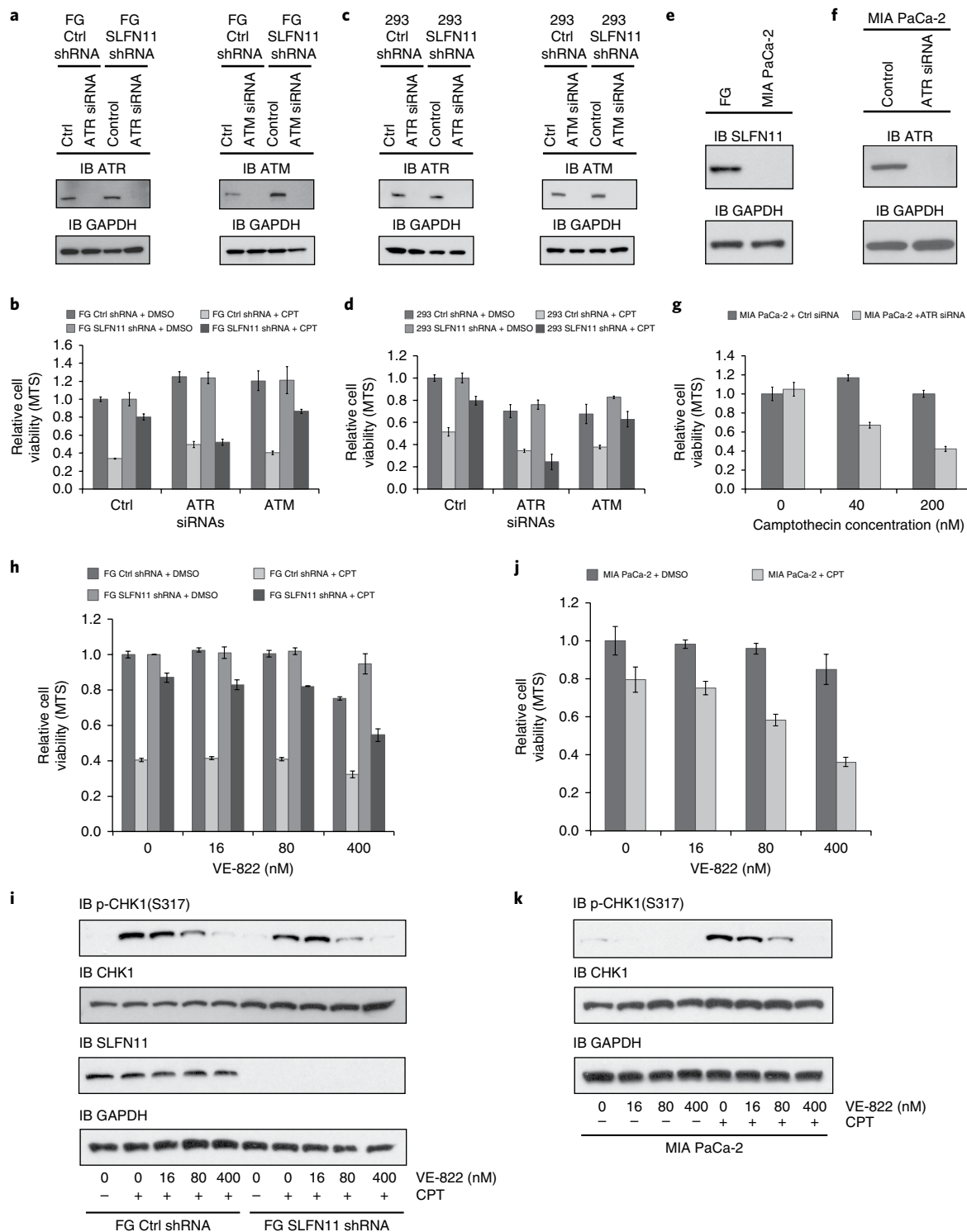


Fig. 2 | Selective inhibition of ATR sensitizes SLFN11-deficient cells to CPT treatment. **a**, Efficiency of ATR/ATM knockdown by siRNAs in FG cells was monitored by immunoblotting 5 days after transfection. **b**, 72 h after siRNAs transfection, FG cells expressing Ctrl or SLFN11 shRNA were treated by 200 nM CPT or DMSO for another 48 h. Relative cell viabilities were determined by MTS assay. **c,d**, As in **a,b** except with HEK 293 cells. **e**, SLFN11 expression deficiency in MIA PaCa-2 cells was confirmed by immunoblotting. **f,g**, As in **a,b** except with MIA PaCa-2 cells. **h**, Relative viabilities of FG cells expressing Ctrl or SLFN11 shRNA after 48 h of the ATR inhibitor VE-822 and 40 nM CPT treatment were measured by MTS assay. **i**, Phosphorylation of CHK1 was determined by immunoblotting after 6 h of 40 nM CPT and VE-822 treatment. **j**, As in **h** except with MIA PaCa-2 cells. **k**, As in **i** except with MIA PaCa-2 cells. Samples were collected after 3 h of 40 nM CPT and VE-822 treatment. **b,d** and **g-i**, mean \pm s.d., $n=3$ independent cell cultures). Uncropped images are shown in Supplementary Dataset 1.

CPT treatment in both 293 and FG cells (Fig. 3a, lane 4) compared to their SLFN11-deficient counterparts (Fig. 3a, lane 10). However, the stability of ATR protein did not appear to be affected by CPT or

SLFN11, as evidenced by the relatively stable levels of newly synthesized 35 S-labeled ATR protein in the chase phase of the experiment (Fig. 3a, lanes 2, 3, 5, 6, 8, 9, 11, 12). Indeed, inhibition of ATR

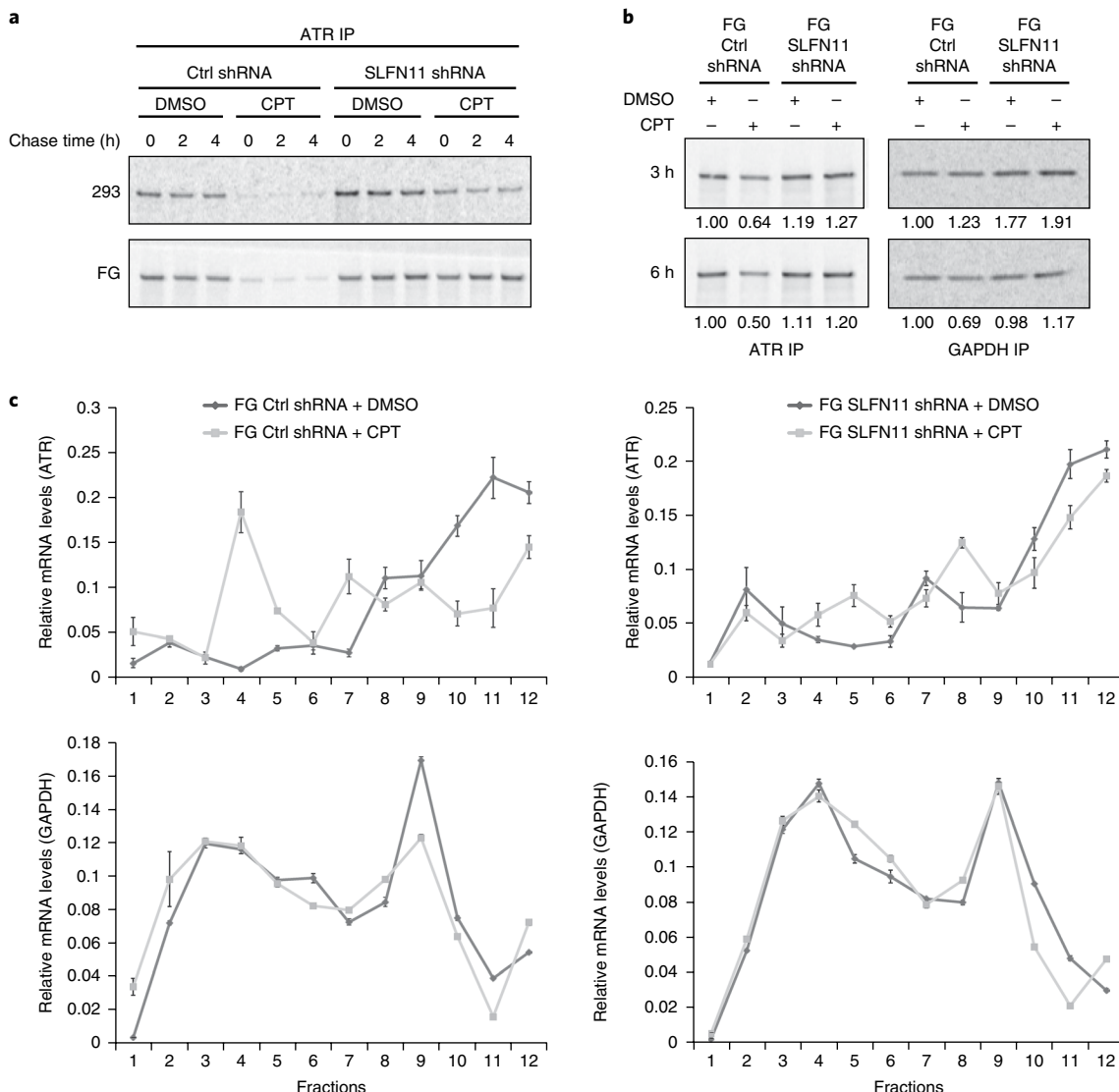


Fig. 3 | SLFN11 selectively inhibits ATR protein synthesis on CPT treatment. **a**, Pulse-chase analysis of ATR protein translation and stability via ^{35}S methionine and ^{35}S cysteine labeling of HEK 293 and FG cells expressing Ctrl or SLFN11 shRNA. Cells were treated with 40 nM CPT or DMSO for 24 h before ^{35}S labeling. **b**, ^{35}S methionine and ^{35}S cysteine protein labeling of FG cells expressing Ctrl or SLFN11 shRNA after 3 or 6 h of 40 nM CPT or DMSO treatment. Numbers indicate quantified band intensity relative to DMSO-treated cells expressing Ctrl shRNA. **c**, Polysome profiles of ATR and GAPDH in FG cells expressing Ctrl or SLFN11 shRNA. Cells were collected and analyzed after 6 h after of DMSO or 40 nM CPT treatment (mean \pm s.d., $n=3$ technical replicates). Uncropped images are shown in Supplementary Dataset 1.

protein synthesis, but not that of GAPDH, was observed as early as 3 h after CPT administration uniquely in SLFN11-expressing cells (Fig. 3b). After 6 h of CPT treatment, slight inhibition of GAPDH translation was observed, while the inhibition of ATR protein synthesis consistently escalated (Fig. 3b). Moreover, polysome profiling experiments also showed that 6 h after CPT treatment was initiated, the ATR polysome profile changed much more substantially in SLFN11-expressing FG cells than in SLFN11-deficient FG cells. Importantly, only minor changes were observed in the GAPDH polysome profile on CPT treatment, regardless of the presence of SLFN11 (Fig. 3c). Altogether, these results demonstrate that on CPT treatment, a prominent inhibition of ATR protein synthesis occurs quickly following DNA damage.

To facilitate our further investigation of the molecular mechanism of SLFN11 function, we established SLFN11-deficient FG and 293 cell lines using CRISPR–Cas9 technology. Complete abrogation of SLFN11 expression via CRISPR–Cas9 yielded an even more

profound phenotype of DDA resistance in both FG and 293 cells (Fig. 4a–d) without substantial effects on cell proliferation in the absence of DDAs (Fig. 4e). A significant increase of caspase 3/7 activity in the presence of SLFN11 on CPT treatment (Fig. 4f), as well as shrinkage of cells and generation of apoptotic bodies (Fig. 4g), further suggest SLFN11 expression sensitizes cells to apoptosis on CPT treatment.

Our prior report of codon usage-dependent, selective translational inhibition of HIV-1 proteins provided initial evidence that SLFN11 affects cellular transfer RNA (tRNA) levels, particularly in infected cells¹. We further investigated whether SLFN11 would potentially alter tRNA levels during the DNA damage response. The 70–87-nucleotide-long tRNAs can be divided into two groups based on the structure and size of their variable loops: tRNAs with a short variable loop of 4 or 5 nucleotides are classified as type I, whereas those harboring a long variable stem, totaling 13–19 bases, are referred to as type II tRNAs. In human cells, the longer type II

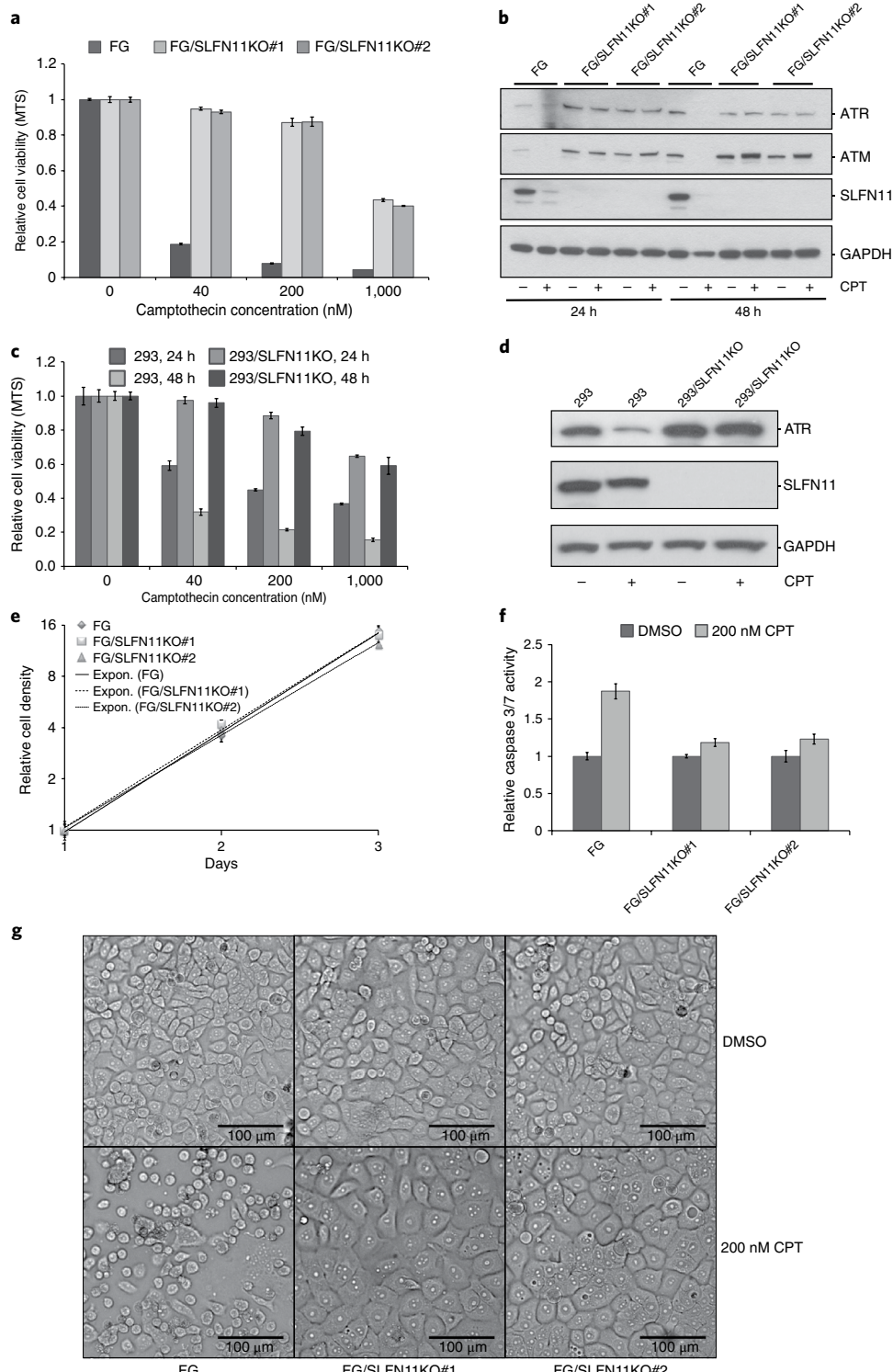


Fig. 4 | CRISPR-Cas9 mediated SLFN11 gene knockout confers significant resistance to CPT-induced apoptosis on cells without affecting cell proliferation. **a**, Relative viability of FG and FG SLFN11 knockout cells was measured by MTS assay after 48 h of CPT or DMSO treatment (mean \pm s.d., $n=3$ independent cell cultures). **b**, Knockout of SLFN11 expression in FG cells by CRISPR-Cas9 technique and its effect on ATR/ATM protein expression on 40 nM CPT or DMSO treatment as determined by immunoblotting. **c**, As in **a** except with HEK 293 cells. **d**, As in **b** except with HEK 293 cells. Cells were analyzed after 24 h of 40 nM CPT or DMSO treatment. **e**, Proliferation of FG and FG SLFN11 knockout cells. **f**, Relative caspase 3/7 activity after 24 h CPT treatment. **g**, Microscopic images of cell cultures after 24 h CPT treatment. Uncropped images are shown in Supplementary Dataset 1.

tRNAs comprise all leucine tRNAs including Leu-AAG, Leu-CAA, Leu-CAG, Leu-TAA and Leu-TAG, and all serine tRNAs including Ser-AGA, Ser-CGA, Ser-GCT and Ser-TGA^{14,15}.

Unexpectedly, analysis of total tRNA abundance revealed that as early as 3 h after CPT treatment was initiated, the levels of type II tRNAs in FG cells already began to decline in a SLFN11-dependent

manner (Fig. 5a,b). After 12 h of CPT treatment, only ~50% of type II tRNAs were still present in SLFN11-expressing FG and 293 cells, whereas no such change was observed in their SLFN11-deficient counterparts. Strikingly, expression levels of type I tRNAs appeared unaffected in response to the DDA regardless of SLFN11 expression (Fig. 5a–d). Similar downregulation of type II tRNAs was also observed on mitoxantrone, gemcitabine or chlorambucil treatment in SLFN11-expressing FG cells (Fig. 5e,f). We additionally performed protein domain function analysis by expressing either the full-length, truncated N-terminal half (amino acid residues 1–579) or C-terminal half (amino acid residues 523–901) of SLFN11 in HEK 293T cells, which is distinguished from its parental cell line HEK 293 in that it lacks endogenous SLFN expression¹. The result clearly indicated that the N-terminal half of SLFN11 contains the effector domain that suppresses type II tRNA levels (Fig. 5g–i).

To identify the individual tRNAs that are downregulated on CPT treatment in the presence of SLFN11, we performed quantitative reverse transcription PCR-based microarray analysis on all nuclear-encoded tRNAs. The tRNAs were first demethylated using *Escherichia coli* alpha-ketoglutarate-dependent dioxygenase (AlkB) to allow efficient reverse transcription of tRNAs, following a protocol that we optimized based on two recent reports^{16,17}. The quantitative PCR (qPCR)-based microarray analysis demonstrated that all leucine tRNAs, as well as Ser-AGA, Ser-TGA and Ser-GGA tRNAs, were significantly downregulated after 12 h of CPT treatment in SLFN11-expressing FG cells (Fig. 6a and Supplementary Dataset 2). Intriguingly, the only type I tRNA also affected was the initiator methionine tRNA Ini-CAT, whose complementary AUG codon represents the classical translation initiation site for most mRNAs^{18,19}. However, most important for our investigation was the finding that not a single tRNA, regardless of its type, was subdued in response to CPT in the absence of SLFN11 (Fig. 6b and Supplementary Dataset 3).

Since the qPCR-based microarray evaluation is a novel, as yet unpublished method of tRNA quantification, we confirmed our findings by northern blot analyses. These assays revealed once again that downregulation of tRNAs Leu-TAA, Leu-CAA, Leu-CAG, Ser-AGA and Ini-CAT began as early as 3 h after CPT administration, followed by a decrease in Leu-TAG, Leu-AAG, Ser-CGA, Ser-GCT and Ser-TGA tRNAs 3 h later (Fig. 6c). Once more, attenuation of these tRNAs was evident only in cells expressing SLFN11 (Fig. 6c).

To further evaluate whether the specific type II tRNA suppression during the DNA damage response was the direct result of SLFN11 activation, we transiently expressed SLFN11 in SLFN11-deficient HEK 293T cells. As shown in Fig. 6d, exogenous expression of SLFN11 alone was sufficient to reduce the levels of all type II serine and leucine tRNAs as well as tRNA Ini-CAT, whereas the type I tRNAs Thr-TGT and Val-TAC remained unchanged. Extended exposure of the tRNA northern blots visualized a fragment of corresponding type II tRNAs in CPT-treated, SLFN11-expressing FG cells, suggesting the SLFN11-mediated reduction of type II tRNAs on CPT treatment is probably the result of direct cleavage of tRNAs (Fig. 6e). The direct cleavage model is also supported by the rapid decline of type II tRNAs immediately after CPT treatment started.

Our data thus far clearly illustrated that all leucine and serine tRNAs are targets of SLFN11. Therefore, we further investigated a possible selective impact of SLFN11 on the translation of genes adopting corresponding codons. To address this point, we designed a series of eGFP-encoding vectors in which each individual construct all leucine or serine residues were encoded by a single codon, with the original EGFP construct as the control. Each construct was then tested by transfection into SLFN11-deficient HEK293T cells, either with or without co-transfection of SLFN11-encoding vector. As demonstrated previously¹, expression of the original EGFP protein was refractory to suppression by SLFN11 (Fig. 6f, lanes 1 and 2, both upper and lower panels). Remarkably, SLFN11 completely

abolished expression of enhanced green fluorescent protein (eGFP) eGFP_Leu(TTA), and to a lesser extent of eGFP_Leu(CTT); eGFP protein derived from all other constructs exhibited marginal or no alteration on account of the presence of SLFN11 (Fig. 6f). Most importantly, the observed inhibition of specific eGFP expression occurred at the translational level, since SLFN11 did not significantly affect the level of eGFP mRNA regardless of the deriving construct (Fig. 6g).

We showed that moderate downregulation of tRNA-Leu-TAA by SLFN11 could inhibit the protein expression of genes with a high frequency of codon TTA (Leu) usage, such as ATR. Since siRNA-mediated knockdown of ATR expression sensitized the SLFN11-deficient cells to DDA, we wondered whether knockdown of tRNA-Leu-TAA would downregulate ATR protein expression and thus sensitize SLFN11-deficient cells to DDA also. Due to the heavy modification and extensive secondary structures of tRNAs, efficient knockdown of specific tRNAs via either siRNAs or shRNAs presents a substantial technical challenge. Therefore, we used a novel antisense oligonucleotide technique called gapmer^{20,21} to design specific gapmers targeting all four tRNA-Leu-TAA isodecoders. Gratifyingly, anti-tRNA-Leu-TAA gapmers downregulated the level of tRNA-Leu-TAA in both FG and FG-SLFN11KO cells, leading to profound inhibition of ATR protein expression (Fig. 7a). Interestingly, although anti-tRNA-Leu-TAA gapmer transfection alone triggered strong caspase 3/7 activation (Fig. 7b), much more substantial cell death was observed only when the anti-tRNA-Leu-TAA gapmer transfected FG-SLFN11KO cells were treated by CPT sequentially, as evidenced by the MTS assay (3-(4,5-dimethylthiazol-2-yl)-5-(3-carboxymethoxyphenyl)-2-(4-sulfophenyl)-2H-tetrazolium) and microscopic imaging of live cell cultures (Fig. 7c,d). The knockdown of tRNA-Leu-TAA by the corresponding gapmer was quite specific; it had only a minor effect on tRNA-Ser-CGA, which was partially targeted by the anti-tRNA-Leu-TAA gapmer (11 nt out of total 16 nt of gapmer Leu-TAA align with most Ser-CGA tRNA isodecoders). Similar results were obtained in intrinsically SLFN11-deficient MIA PaCa-2 cells (Fig. 8a–d).

Discussion

DDAs are the earliest and most widely used therapeutics for cancer treatment, accounting for almost one third of all chemotherapeutic drugs. However, many tumors are resistant to therapies based on DNA-damaging approaches. Even tumors that are initially responsive to the regimen routinely acquire resistance over the course of the treatment (reviewed in Cheung-Ong et al.²²). Two large-scale transcriptome profiling approaches revealed a clear requirement of SLFN11 in cancer cells for DDAs to trigger cell death^{2,3}. Most recently, a study showed that, in recurring small cell lung cancer, silencing of SLFN11 expression mediated by histone H3K27me3 modification at the SLFN11 gene locus was responsible for the tumor's acquired chemoresistance. Inhibition of histone-lysine N-methyltransferase EZH2 restored SLFN11 expression and resensitized the tumor cells to chemotherapy²³. We found that early DNA damage response signals, such as the phosphorylation of CHK1, are not affected by SLFN11 expression; this is consistent with other reports that SLFN11 does not change early DNA damage responses but inhibits checkpoint maintenance and homologous recombination repair at the later stages. It was suggested that SLFN11 is promptly recruited to the sites of DNA damage via replication factor A protein 1 (RPA1)²⁴, which could be a step in the as yet unknown activation mechanism of SLFN11. A recent independent study also reported that, on CPT treatment, SLFN11 is promptly recruited to chromatin at stressed replication foci via RPA1, but does not affect the early DNA damage response signaling event, such as phosphorylation of CHK1, or the loading of CDC45 and proliferating cell nuclear antigen²⁵.

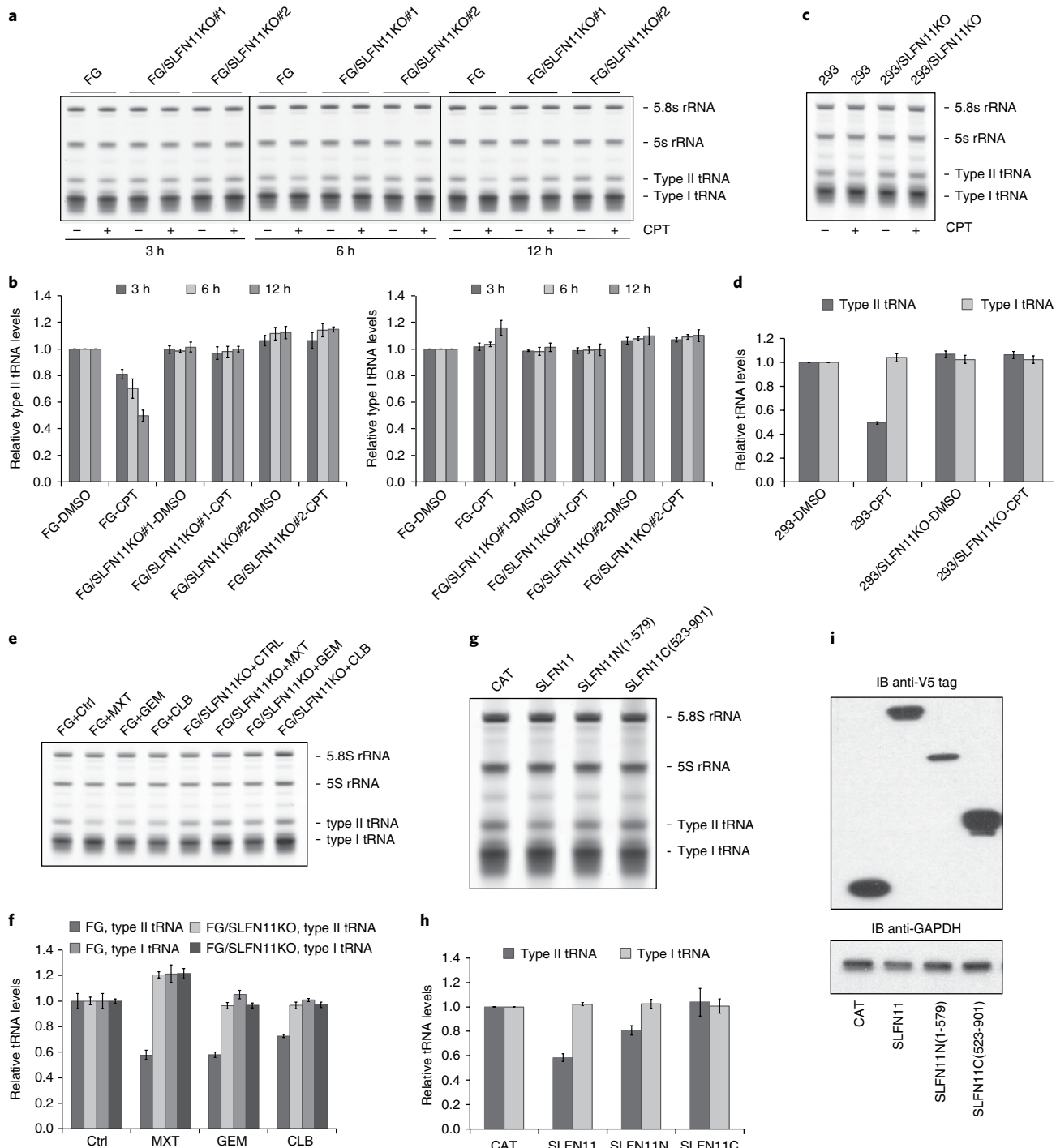


Fig. 5 | SLFN11 mediates the downregulation of type II tRNAs on DDA treatment. **a**, Total RNAs from FG and FG SLFN11 knockout cells treated with 200 nM CPT or DMSO were resolved by 10% denaturing urea PAGE, visualized by SYBR Gold staining and quantified. **b**, Quantified results from **a** (error bars are mean \pm s.d., $n=3$ independent cell cultures; 5.8S rRNA served as the endogenous control for normalization; all data are presented relative to DMSO-treated FG cell samples). **c**, As in **a** except with HEK 293 cells. Cells were analyzed after 12 h of 200 nM CPT or DMSO treatment. **d**, As in **b**, quantified results from **c**. **e**, As in **a**, FG and FG SLFN11 knockout cells were treated with mitoxantrone (MXT, 1 μ M), gemcitabine (GEM, 1 μ M), chlorambucil (CLB, 100 μ M) or DMSO for 12 h. **f**, As in **b**, quantified results from **e**. **g**, Total RNAs from HEK 293T cells exogenously expressing V5-tagged chloramphenicol acetyl transferase (CAT), SLFN11, SLFN11N (amino acid residues 1–579) or SLFN11C (amino acid residues 523–901) were collected 48 h after transfection and analyzed as in **a**. **h**, As in **b**, quantified results from **g**. **i**, Expression levels of the corresponding SLFN11 proteins was confirmed by immunoblotting against the V5 tag. Uncropped images are shown in Supplementary Dataset 1.

In this article, we describe a novel molecular mechanism by which SLFN11 sensitizes cells to apoptosis upon DNA damage. The SLFN11-dependent downregulation of type II tRNAs, most

importantly tRNA-Leu-TAA, predisposes genes that are essential for the DNA damage response and repair, such as ATR or ATM, to translational inhibition as they use the corresponding codon TTA

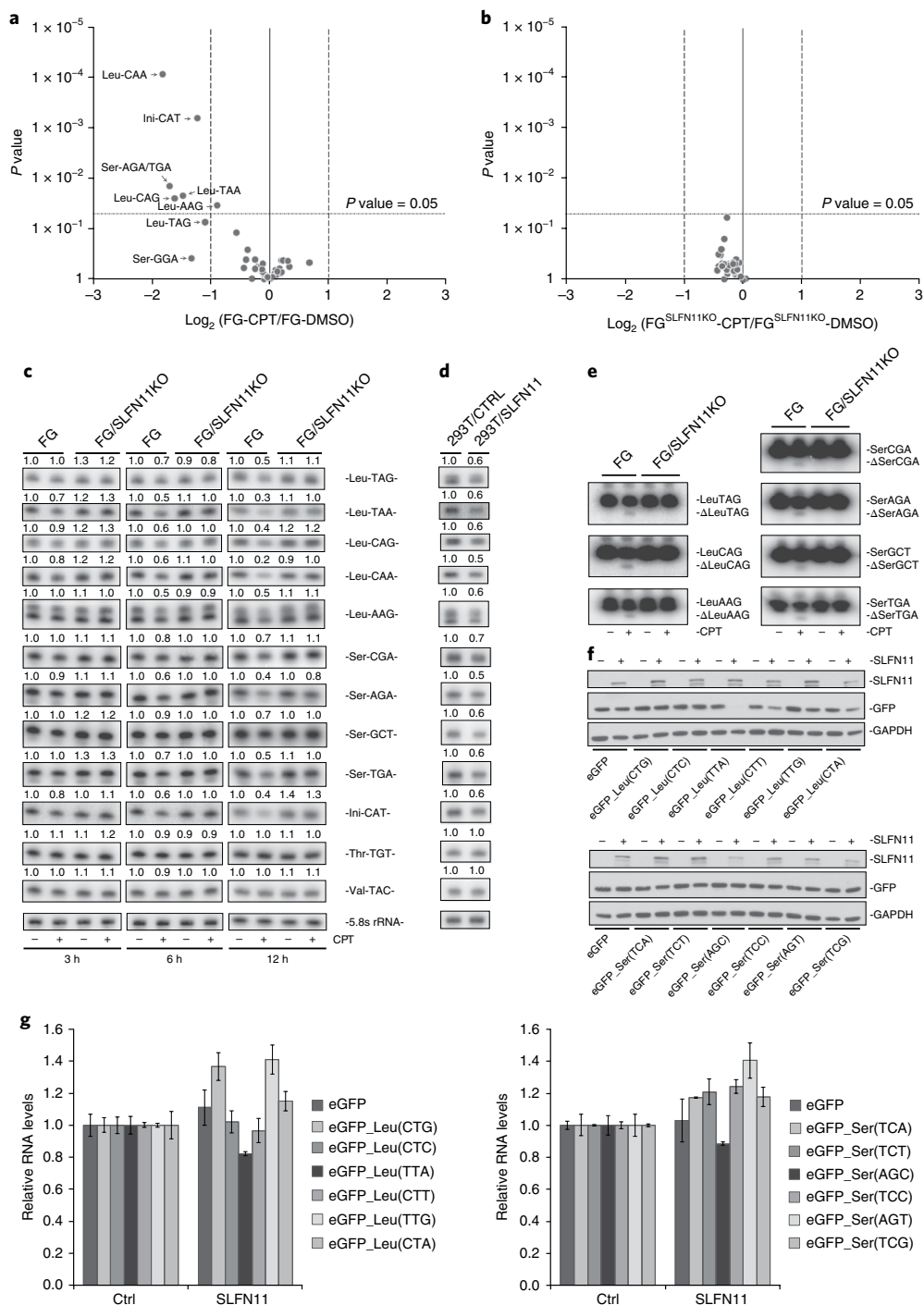


Fig. 6 | SLFN11-mediated type II tRNAs cleavage inhibits mRNA translation of genes with high frequency of codon TTA (Leu) usage. **a**, Volcano plot of fold change of all cellular tRNAs after 12 h of 200 nM CPT or DMSO treatment in FG cells as determined by qPCR. **b**, as in **a** except in FG SLFN11 knockout cells. \log_2 (mean of fold change) versus P value; $n=3$ independent cell cultures; the P value was calculated by performing a two-tailed, two-sample equal variance (homoscedastic) Student's t -test. **c**, tRNA northern blot analysis of total RNA isolated from FG and FG SLFN11 knockout cells treated with 200 nM CPT or DMSO. **d**, tRNA northern blot analysis of total RNA from HEK 293T cells exogenously expressing control protein (CAT) or SLFN11. Samples were collected 48 h after transfection. Numbers indicate quantified band intensity relative to DMSO-treated FG cell samples in **c** or relative to CAT-expressing HEK 293T cell controls in **d**; 5.8S rRNA served as the endogenous control for normalization. **e**, Prolonged exposure of tRNA northern blots of total RNA from FG and FG SLFN11 knockout cells treated with 200 nM CPT or DMSO for 12 h, revealing the cleaved tRNA fragments. **f**, Protein expression of eGFP encoded by constructs using only the indicated codon for all leucine or serine residues in HEK 293T cells in the absence or presence of exogenous SLFN11 expression 48 h after transfection as determined by anti-GFP immunoblotting. **g**, As in **f**, relative mRNA levels derived from indicated eGFP constructs were determined by qPCR ($\text{mean} \pm \text{s.d.}$; $n=3$ independent cell cultures). Uncropped images are shown in Supplementary Dataset 1.

(Leu). At the onset of this study, we noted that synthesis of proteins encoded by genes with a low CAI resembling that of HIV were drastically more repressed by SLFN11 than the translation of genes with

high CAI. The overall TTA (Leu) codon usage frequency is only about 8% for the human genome coding sequences, and 2% for the 24 most highly expressed human cellular proteins (Supplementary

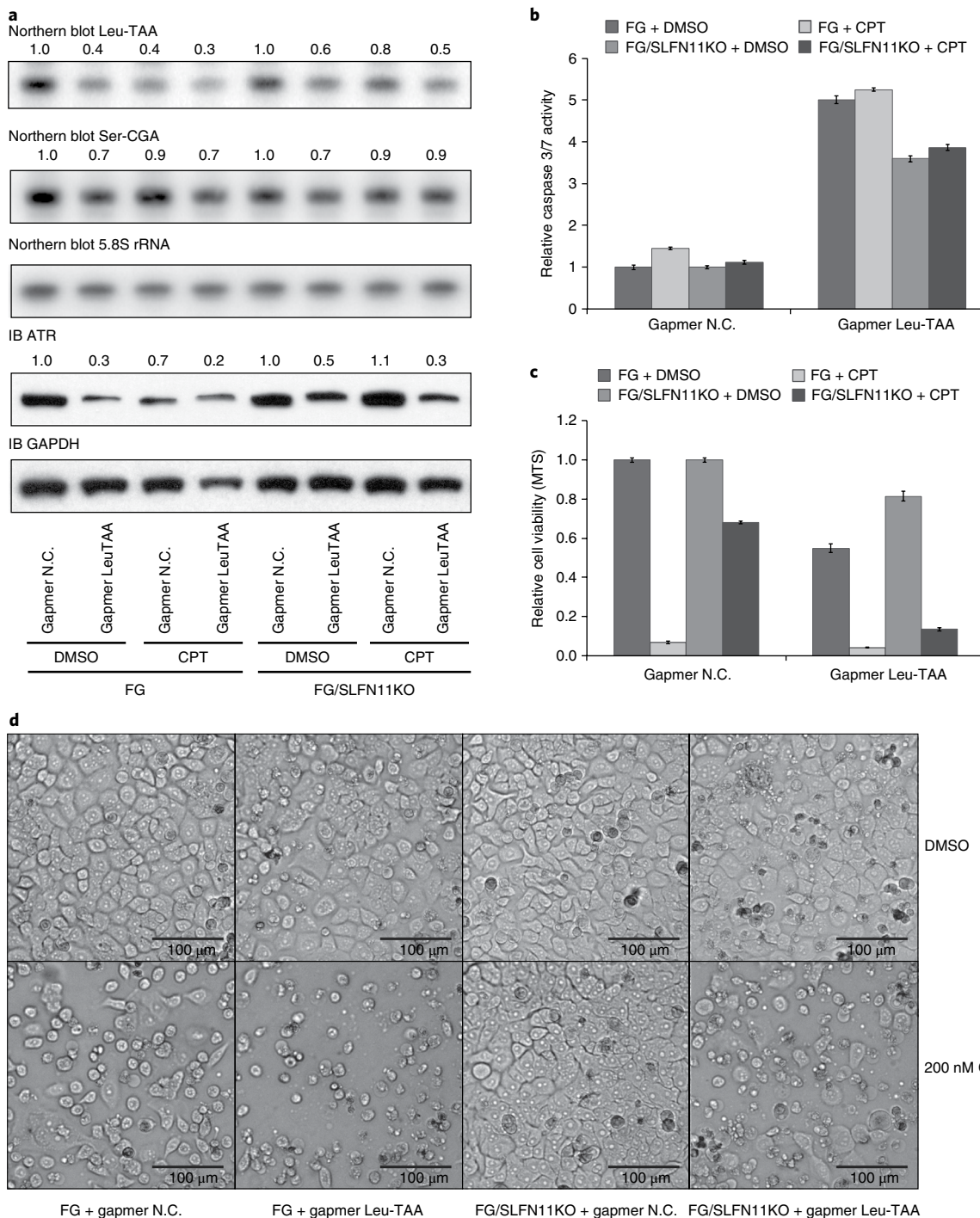


Fig. 7 | Ablation of tRNA-Leu-TAA via gapmer antisense oligonucleotides resensitizes SLFN11-deficient FG cells to CPT-induced apoptosis. 12 h after transfection with control gapmer (N.C.) or a gapmer specific for tRNA-Leu-TAA (50 nM), FG and FG SLFN11 knockout cells were treated with DMSO or 200 nM CPT. **a**, Total RNA was collected 12 h after CPT treatment and subjected to northern blot analysis. Protein for immunoblotting was collected 24 h after CPT treatment. Numbers represent quantified band intensity relative to DMSO-treated, gapmer N.C.-transfected cell samples. 5.8S rRNA served as the control for the northern blot. GAPDH served as the control for immunoblotting. **b**, Relative caspase 3/7 activity after 12 h CPT treatment. **c**, Relative cell viabilities after 60 h CPT exposure were measured by MTS assay (**b,c** mean \pm s.d., $n=3$ independent cell cultures). Both are relative to DMSO-treated, gapmer N.C.-transfected cell samples. **d**, Microscopic images of cell cultures after 24 h CPT treatment. Uncropped images are shown in Supplementary Dataset 1.

Table 4). In striking contrast, genes involved in HDR, NHEJ and MMR display much higher average TTA (Leu) codon usage (18, 15 and 13%, respectively), even when compared to genes affiliated with NER and BER (9 and 6%, respectively) (Supplementary Tables 5 and 6). Indeed, out of the 352 leucines in ATR, 73 use the codon

TTA (21%), and of 389 leucine residues in ATM, 91 are encoded by TTA (23%). In striking contrast, only a single TTA codon is found among the 19 leucine residues of GAPDH (5%). Our previous work demonstrated that the distinct codon bias facilitates preferential translational inhibition of HIV proteins by SLFN11. We now show

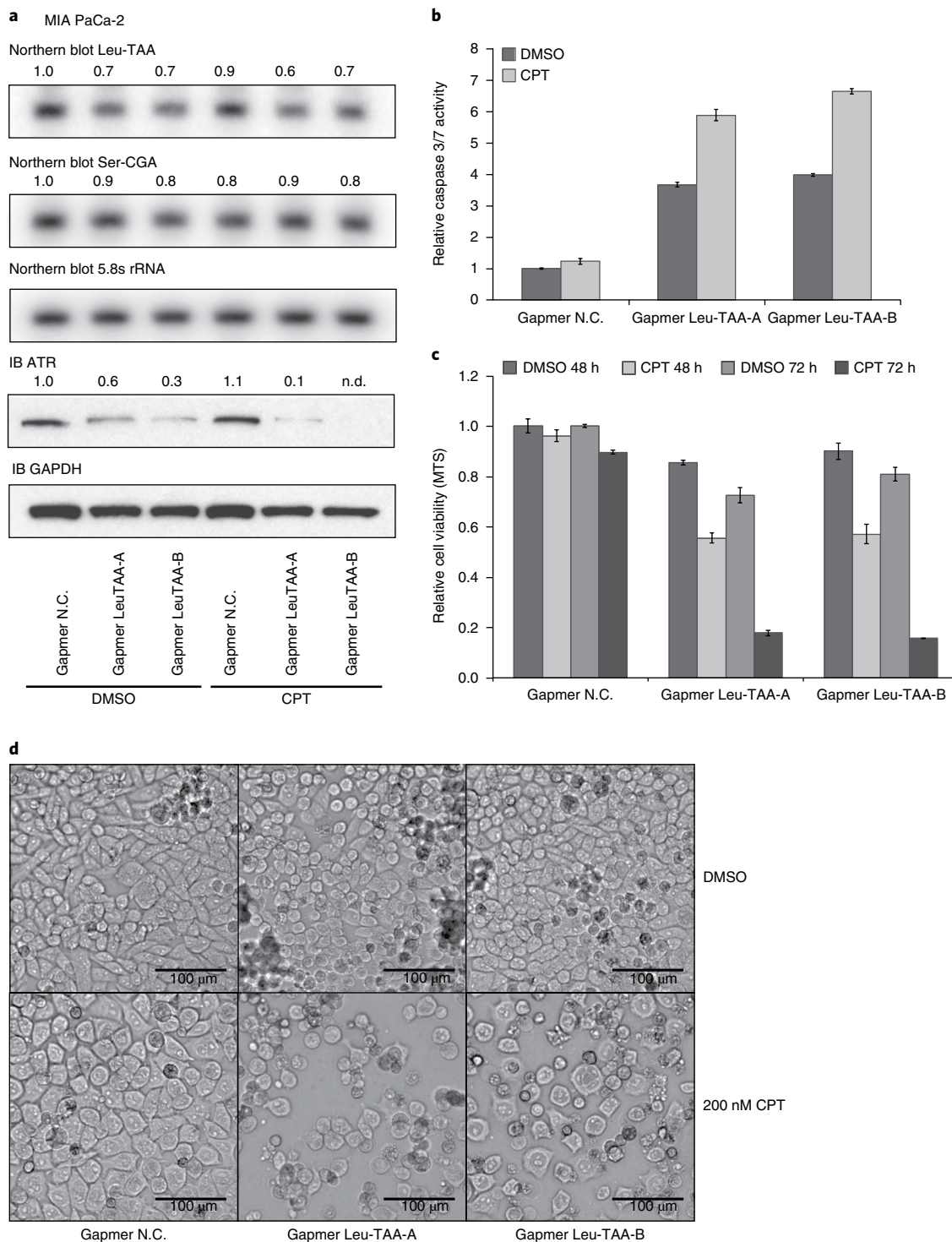


Fig. 8 | Gapmer antisense oligonucleotides directed at tRNA-Leu-TAA sensitize intrinsically SLFN11-deficient MIA PaCa-2 cells to CPT-induced apoptosis. 12 h after transfection with control gapmer (N.C.) or gapmers against tRNA-Leu-TAA (12.5 nM), MIA PaCa-2 cells were treated with DMSO or 200 nM CPT. **a**, Total RNA for northern blots was collected after 12 h CPT treatment. Protein samples for immunoblotting were collected after 36 h CPT treatment. Numbers indicate quantified band intensity relative to DMSO-treated, gapmer N.C.-transfected control cell samples. 5.8S rRNA served as control for the northern blots. GAPDH served as control for immunoblotting. **b**, Relative caspase 3/7 activity was measured after 24 h CPT treatment. **c**, 48 or 72 h after CPT exposure, relative cell viabilities were determined by MTS assay (**b,c**, error bars indicate mean \pm s.d., $n=3$ independent cell cultures; both relative to DMSO-treated, gapmer N.C.-transfected control cell samples). **d**, Microscopic images of cell cultures after 24 h CPT treatment. Uncropped images are shown in Supplementary Dataset 1.

that select mammalian genes, such as those associated with DNA damage response signaling (for example, ATR or ATM), harbor a similar codon usage distinction as HIV. Our more detailed analysis

reveals that the frequency of TTA (Leu) codon usage is the apparent common denominator that subjects the encoded proteins to translational suppression by SLFN11 (Supplementary Table 4).

An outstanding question to be addressed in future is why only SLFN11-mediated degradation of tRNA-Leu-TAA affects the translation efficiency of mRNAs harboring the corresponding codon, whereas the cleavage of other leucine or serine tRNAs appears to be of lesser consequence. One possible explanation is the apparently lower abundance of tRNA-Leu-TAA (for codon TTA) that we have noted in our qPCR and northern blot analyses. Although neither technique permits a highly accurate quantitative assessment, they support a reasonable estimation of relative tRNA abundance. For instance, the qPCR cycle threshold (C_t) value for tRNA-Leu-CAG (for codon CTG) was about four cycles lower than the C_t value of tRNA-Leu-TAA (for codon TTA), suggesting the abundance of tRNA-Leu-CAG is roughly 16-fold higher than that of tRNA-Leu-TAA. A similar observation was reflected by the relative signal intensity in our northern blot analysis. Thus, for gene products requiring tRNA-Leu-TAA to support their translation, the availability of this tRNA may readily become the rate-limiting factor, and a consequent downregulation of tRNA-Leu-TAA may cause the ribosome to stall and/or detach at the corresponding TTA codons. This effect is expected to be amplified with the increased frequency of the TTA codon and with the length of the mRNA, with the end result that the longer the mRNA and higher the frequency of TTA codon usage for leucine residues increases the probability that premature translation termination will occur. In contrast, the translation rates for proteins that rely on more abundant, synonymous tRNAs will not be significantly affected by the reduced but nevertheless sufficient supply of required tRNAs.

Our present data show that the N-terminal half (amino acid residues 1–579) of human SLFN11 comprises the functional domain responsible for the degradation of type II tRNAs. It was reported that a leporine SLFN14 N-terminal fragment in rabbit reticulocyte lysate harbors endoribonuclease activity²⁶. Furthermore, the crystallographic structure of the murine SLFN13 N-terminal domain (amino acid residues 14–353) was recently determined and shown to possess intrinsic tRNA and ribosomal RNA (rRNA)-targeting endoribonuclease activity *in vitro*²⁷. In concert with our own studies, these findings firmly establish SLFN family members as a novel class of tRNA-specific endoribonucleases with the enzymatic activity residing in an N-terminal protein domain with an apparent specificity for type II tRNAs.

Mu et al.²⁴ reported that an SLFN11 deletion mutant lacking the extreme C-terminal sequence (amino acid residues 741–901) could not bind to RPA1 and was not recruited to DNA damage sites. This C-terminal deletion mutant also failed to resensitize SLFN11-deficient cells to CPT. In contrast, we found that further deletion variants that retain only the N-terminal half of SLFN11 (amino acid residues 1–579) can degrade type II tRNAs, and, as we have previously shown, attenuate the translation of HIV proteins. One possible explanation for these findings is that the C-terminal half of SLFN11 acts as a regulatory domain with auto-inhibitory properties that are relieved by posttranslational modifications, which may occur at the sites of DNA damage. A short truncation as in Mu et al.²⁴ could possibly remove the site required for activation, but still retain enough of the C-terminal domain to inhibit such truncated SLFN11. However, the more extensive deletion that we employed may fully remove such inhibitory elements, and thus result in an active, albeit unregulated, SLFN11 fragment harboring a newly discovered tRNAse activity. In addition to the potential activation mechanisms of SLFN11, the subcellular location where it exerts its tRNA-degrading effects also requires further investigation. Although mature tRNAs generally function outside the nucleus, they move between the cytoplasm and the nucleus dynamically²⁸, and thus may be susceptible to cleavage by SLFN11 regardless of their subcellular localization.

Although the cleavage of type II tRNAs by SLFN11, and consequent ATR suppression, are undoubtedly crucial components

of DDA-induced cell death, our observations do not preclude the possibility that additional aspects of the DNA damage response are affected by SLFN11. Our studies do not rule out the possibility that induction of chromatin opening across replication initiation sites and blocking of fork progression by SLFN11 on CPT treatment may be an additional mechanism of SLFN11 function. However, as we show in this study, tRNA-Leu-TAA degradation with specifically targeted gapmers is sufficient to restore DNA damage-induced apoptosis via CPT in SLFN11-deficient cells, suggesting that this step is a crucial element of SLFN11 function.

In summary, our findings not only provide new insights into the molecular mechanism underlying SLFN11 function, but reveal that modulation of distinct tRNAs facilitates the specific targeting of proteins that rely on those tRNAs for their translation. The technical difficulty of manipulating specific tRNA expression has been a substantial obstacle to elucidating the role of tRNA levels and their contribution to the regulation of gene expression. In this article, we demonstrate for the first time that gapmer technology can be used to specifically attenuate the levels of individual tRNAs. The direct targeting of tRNA-Leu-TAA offers a new strategy to overcome tumor cell resistance to DDAs, and may hold unanticipated clinical potential.

URLs. ImageJ, <https://imagej.nih.gov/ij/>; GtRNAdb, tRNAscan-SE analysis of complete genomes, <http://gtrnadb.ucsc.edu>.

Online content

Any methods, additional references, Nature Research reporting summaries, source data, statements of data availability and associated accession codes are available at <https://doi.org/10.1038/s41594-018-0142-5>.

Received: 16 May 2018; Accepted: 7 September 2018;
Published online: 29 October 2018

References

- Li, M. et al. Codon-usage-based inhibition of HIV protein synthesis by human schlafen 11. *Nature* **491**, 125–128 (2012).
- Zoppoli, G. et al. Putative DNA/RNA helicase Schlafen-11 (SLFN11) sensitizes cancer cells to DNA-damaging agents. *Proc. Natl Acad. Sci. USA* **109**, 15030–15035 (2012).
- Barretina, J. et al. The Cancer Cell Line Encyclopedia enables predictive modelling of anticancer drug sensitivity. *Nature* **483**, 603–607 (2012).
- Schwarz, D. A., Katayama, C. D. & Hedrick, S. M. Schlafen, a new family of growth regulatory genes that affect thymocyte development. *Immunity* **9**, 657–668 (1998).
- Bustos, O. et al. Evolution of the Schlafen genes, a gene family associated with embryonic lethality, meiotic drive, immune processes and orthopoxvirus virulence. *Gene* **447**, 1–11 (2009).
- Sharp, P. M. & Li, W. H. The codon Adaptation Index: a measure of directional synonymous codon usage bias, and its potential applications. *Nucleic Acids Res.* **15**, 1281–1295 (1987).
- Puigbò, P., Bravo, I. G. & Garcia-Vallve, S. CAIcal: a combined set of tools to assess codon usage adaptation. *Biol. Direct.* **3**, 38 (2008).
- Jalal, S., Earley, J. N. & Turchi, J. J. DNA repair: from genome maintenance to biomarker and therapeutic target. *Clin. Cancer Res.* **17**, 6973–6984 (2011).
- Brown, J. S., O’Carrigan, B., Jackson, S. P. & Yap, T. A. Targeting DNA repair in cancer: beyond PARP inhibitors. *Cancer Discov.* **7**, 20–37 (2017).
- Beck, M. et al. The quantitative proteome of a human cell line. *Mol. Syst. Biol.* **7**, 549 (2011).
- Blackford, A. N. & Jackson, S. P. ATM, ATR, and DNA-PK: the trinity at the heart of the DNA damage response. *Mol. Cell* **66**, 801–817 (2017).
- Cimprich, K. A. & Cortez, D. ATR: an essential regulator of genome integrity. *Nat. Rev. Mol. Cell Biol.* **9**, 616–627 (2008).
- Morgan, R. T. et al. Human cell line (COLO 357) of metastatic pancreatic adenocarcinoma. *Int. J. Cancer* **25**, 591–598 (1980).
- Chan, P. P. & Lowe, T. M. GtRNAdb: a database of transfer RNA genes detected in genomic sequence. *Nucleic Acids Res.* **37**, D93–D97 (2009).
- Chan, P. P. & Lowe, T. M. GtRNAdb 2.0: an expanded database of transfer RNA genes identified in complete and draft genomes. *Nucleic Acids Res.* **44**, D184–D189 (2016).

16. Zheng, G. et al. Efficient and quantitative high-throughput tRNA sequencing. *Nat. Methods* **12**, 835–837 (2015).
17. Cozen, A. E. et al. ARM-seq: AlkB-facilitated RNA methylation sequencing reveals a complex landscape of modified tRNA fragments. *Nat. Methods* **12**, 879–884 (2015).
18. Hinnebusch, A. G. Molecular Mechanism of Scanning and Start Codon Selection in Eukaryotes. *Microbiol. Mol. Biol. Rev.* **75**, 434–467 (2011).
19. Kolitz, S. E. & Lorsch, J. R. Eukaryotic initiator tRNA: finely tuned and ready for action. *FEBS Lett.* **584**, 396–404 (2010).
20. Grünweller, A. et al. Comparison of different antisense strategies in mammalian cells using locked nucleic acids, 2'-O-methyl RNA, phosphorothioates and small interfering RNA. *Nucleic Acids Res.* **31**, 3185–3193 (2003).
21. Kurreck, J., Wyszko, E., Gillen, C. & Erdmann, V. A. Design of antisense oligonucleotides stabilized by locked nucleic acids. *Nucleic Acids Res.* **30**, 1911–1918 (2002).
22. Cheung-Ong, K., Giaever, G. & Nislow, C. DNA-damaging agents in cancer chemotherapy: serendipity and chemical biology. *Chem. Biol.* **20**, 648–659 (2013).
23. Gardner, E. E. et al. Chemosensitive relapse in small cell lung cancer proceeds through an EZH2-SLFN11 axis. *Cancer Cell* **31**, 286–299 (2017).
24. Mu, Y. et al. SLFN11 inhibits checkpoint maintenance and homologous recombination repair. *EMBO Rep.* **17**, 94–109 (2016).
25. Murai, J. et al. SLFN11 blocks stressed replication forks independently of ATR. *Mol. Cell* **69**, 371–384.e6 (2018).
26. Pisareva, V. P., Muslimov, I. A., Tcherepanov, A. & Pisarev, A. V. Characterization of novel ribosome-associated endoribonuclease SLFN14 from rabbit reticulocytes. *Biochemistry* **54**, 3286–3301 (2015).
27. Yang, J. Y. et al. Structure of Schlafen13 reveals a new class of tRNA/rRNA-targeting RNase engaged in translational control. *Nat. Commun.* **9**, 1165 (2018).
28. Hopper, A. K. & Huang, H. Y. Quality control pathways for nucleus-encoded eukaryotic tRNA biosynthesis and subcellular trafficking. *Mol. Cell. Biol.* **35**, 2052–2058 (2015).

Acknowledgements

The authors wish to thank R. Lardelli and M. Arribas-Layton for assistance with northern blot and polysome profile analyses. This work was supported by grants R01-GM101982 and R21-AI124199 to M.D.

Author contributions

M.L., J.Y.W. and M.D. conceived the experiments. E.K. and X.G. performed the cell viability studies, ATR experiments and polysome analysis. M.L., X.G. and D.M. are responsible for all tRNA data and codon usage studies. M.L. and X.G. designed and performed all gapmer related studies. M.L., E.K. and D.M. generated the figures. M.L. and M.D. wrote the manuscript.

Competing interests

The authors declare no competing interests.

Additional information

Supplementary information is available for this paper at <https://doi.org/10.1038/s41594-018-0142-5>.

Reprints and permissions information is available at www.nature.com/reprints.

Correspondence and requests for materials should be addressed to M.L. or M.D.

Publisher's note: Springer Nature remains neutral with regard to jurisdictional claims in published maps and institutional affiliations.

© The Author(s), under exclusive licence to Springer Nature America, Inc. 2018

Methods

Cell lines, plasmids, antibodies and chemicals. All cell lines were maintained at 37 °C, 5% CO₂ in high glucose DMEM supplemented with 10% heat-inactivated fetal bovine serum, 100 U ml⁻¹ penicillin, 100 µg ml⁻¹ streptomycin, 2 mM L-Glutamine, 1 × MEM non-essential amino acid, 1 mM sodium pyruvate and 50 µM 2-mercaptoethanol. The HEK 293 and HEK 293T cell lines were acquired from ATCC. Both COLO 357/FG and MIA PaCa-2 cell lines were acquired from Dr. Tannishtha Reya at the University of California, San Diego. HEK 293 and COLO 357/FG cell lines with stable expression of shRNAs were generated using lentivirus-based vectors as previously described¹. To obtain HEK 293 and COLO 357/FG derivative cell lines in which SLFN11 expression was obliterated using the CRISPR-Cas9 technique, cells were transfected with pSpCas9(BB)-2A-Puro (PX459) all-in-one CRISPR-Cas9 construct and selected based on puromycin resistance (for HEK 293 cells: SLFN11 CRISPR-Cas9 guide RNA 4, GCAGCTGACAAACGGAGAAA; for FG cells: SLFN11 CRISPR-Cas9 guide RNA 1, GGCTTGACAGAGCGATCTTC; both were obtained from GenScript). Surviving cells were cloned by limiting dilution and screened for SLFN11 expression by immunoblotting. The construction of the pcDNA6-SLFN11-V5-His and pcDNA6.2-EGFP-Myc expression vectors was previously reported¹. ATR antibody (N-19), CHK1 antibody (G-4), SLFN11 antibody (E-4) and V5-Probe (G-14)-R were obtained from Santa Cruz Biotechnology. Antibodies against ATR, ATM (D2E2), Phospho-CHK1 (Ser317) (D12H3), GFP (D5.1) and GAPDH (14C10) were purchased from Cell Signaling Technology. Antibody for GAPDH immunoprecipitation was acquired from Abcam. Camptothecin was procured from EMD Millipore, mitoxantrone and gemcitabine from Enzo Life Sciences, chlorambucil from MP Biomedicals and the ATR inhibitor VE-822 from Selleck Chemicals.

siRNA transfection. Reverse transfection of cells was performed using ON-TARGETplus SMARTpool siRNAs (Dharmacon) and RNAiMAX reagent (Thermo Fisher Scientific) in 96-well plates; 72 h post-transfection cells were treated with the indicated drugs for 48 h before collection and immunoblotting analysis. The survival rates of siRNA transfected cells were determined by means of MTS-based cell viability assays.

Design and transfection of gapmers. Gapmer antisense oligonucleotides designed to target tRNA sequence regions with fewer secondary structures were synthesized by Exiqon (QIAGEN). An ‘*’ represents a phosphorothioate bond, and ‘+A’, ‘+T’, ‘+G’, ‘+C’ represent corresponding locked nucleic acid residues, respectively. Cells were transfected with gapmers using RNAiMAX (Thermo Fisher Scientific) at the indicated concentrations 24 h after the cells were plated, followed by an additional 12 h of incubation before further treatment. Unless specified otherwise, gapmer tRNA-Leu-TAA-B was used for tRNA-Leu-TAA knockdown because of its lesser cytotoxicity and more potent effect.

Gapmer tRNA-Leu-TAA-A:
+T* + C* + T* + T* A* A* G*T*C*C*A*A* + C* + G* + C* + C
Gapmer tRNA-Leu-TAA-B:
+C* + C* + A* + T*T*G*G*A*T*C*T*T* + A* + A* + G* + T
Gapmer negative control:
+T* + A* + C* + G*C*G*T*C*T*A*T*A* + C* + G* + C* + A

MTS cell viability assay. Cells were seeded in 96-well clear tissue culture plates 24 h before the indicated regimen in complete phenol red-free DMEM medium. MTS was added to the cell culture at the end of the intended treatments according the manufacturer’s protocol (CellTiter 96® AQueous One Solution Cell Proliferation Assay, Promega Corporation). Absorbance was measured at 490 nm after incubation at 37 °C for 2 h.

Caspase 3/7 activity assay. Caspase 3/7 activity was measured with Caspase-Glo 3/7 Assay Systems (Promega Corporation) according the manufacturer’s protocol. Briefly, cells were seeded in 96-well tissue culture plates with a white wall and clear bottom in complete phenol red-free DMEM medium and treated as indicated specifically. An equal volume of Caspase-Glo 3/7 reagent was added into the cell culture and gently mixed using a plate shaker at 600 rpm for 30 s. The plate was incubated at room temperature for 30 min and the generated luminescence signal was measured by a NOVOSTAR (BMG LABTECH) multifunction plate reader.

Whole-cell lysis and immunoblotting. Cells were lysed in 1 × Cell Lysis Buffer (Cell Signaling Technology) supplemented with Phosphatase Inhibitor Cocktail Set I, Phosphatase Inhibitor Cocktail Set II and Protease Inhibitor Cocktail Set III (all EMD Millipore), and 1 mM phenylmethylsulfonyl fluoride. Samples were resolved by 4–12% sodium dodecyl sulfate–polyacrylamide gel electrophoresis (SDS-PAGE; Invitrogen) and transferred onto polyvinylidene difluoride (PVDF) membranes. After incubation with target-specific primary antibody and horseradish peroxidase-conjugated secondary antibody, signals were detected using Western Lightning ECL Pro (PerkinElmer) and film exposure. When needed, the film was scanned and quantified with ImageJ64 (see URLs).

Total RNA preparation and mRNA qPCR. Total cellular RNA was isolated with guanidinium thiocyanate (TRIzol; Invitrogen) and cleaned with the TURBO

DNA-free Kit (Invitrogen Ambion). Reverse transcription was performed using the High Capacity cDNA Reverse Transcription Kit (Thermo Fisher Scientific). The qPCR reactions were carried out on a StepOne Plus Real-Time PCR System (Thermo Fisher Scientific) using the iTaq Universal SYBR Green Supermix (Bio-Rad Laboratories) according the manufacturer’s protocols. The relative levels of mRNAs of interest were calculated based on ΔCt values and subsequent normalization to GAPDH mRNA levels. The following qPCR primers were used in these assays:

ATR forward 5'-CGCTGAACGTACGTGGAAA-3';
ATR reverse 5'-CAATTAGTCCTGGTAAACATC-3';
ATM forward 5'-TTTCTTACAGTAATTGGAGCATTTG-3';
ATM reverse 5'-GGCAATTACTAGGGCCATTG-3';
GAPDH forward 5'-TCCACTGGCGTCTCAC-3';
GAPDH reverse 5'-GGCAGAGATGACCCCTTT-3';
eGFP-tag forward 5'-CGCCGACCCAGCTTCTTGTA-3';
eGFP-tag reverse 5'-TGATCAGCTCTGCTGCCG-3'.

tRNA demethylation and qPCR-based tRNA microarray assay. Total cellular RNA was prepared with TRIzol (Invitrogen), treated with TURBO DNA-free Kit (Thermo Fisher Scientific) and repurified with TRIzol. The tRNA demethylation was carried out following a manufacturer-provided protocol (Arraystar) modified and optimized in our laboratory: 2.5 µg total RNA was incubated with 2.5 µl AlkB demethylase, 1 µl RNasin Plus RNase Inhibitor (Promega) in a total of 100 µl freshly prepared tRNA demethylation buffer (50 mM 2-(N-morpholino)ethanesulfonic acid pH 6.0, 100 mM KCl, 2 mM L-ascorbate, 1 mM α-ketoglutarate, 50 µg ml⁻¹ UltraPure BSA (Thermo Fisher Scientific), 300 µM ammonium Iron(II) sulfate hexahydrate (Fe(NH₄)₂(SO₄)₂·6H₂O)) at 37 °C for 2 h. The reaction was terminated by sequential addition of EDTA and MgCl₂ (final concentration 1 mM each). Total RNA was further purified by phenol-chloroform extraction and isopropanol precipitation. Reverse transcription was performed with the rtStar tRNA-optimized First-Strand cDNA Synthesis Kit (Arraystar); qPCR for all cellular tRNAs was performed with the nrStar Human tRNA Repertoire PCR Array (Arraystar) and SYBR Green qPCR Master Mix (Arraystar) on a QuantStudio 7 Flex Real-Time PCR System (Thermo Fisher Scientific). The data were analyzed with the analysis tool for nrStar Human tRNA repertoire PCR Array, version 1.01 with the cutoff Ct set at 30. The P values were calculated using a two-tailed, two-sample equal variance (homoscedastic) Student’s t-test.

Polysome profiling by sucrose gradient. Cells were seeded 24 h before 6 h treatment with DMSO or 40 nM CPT, subsequently incubated with 100 µg ml⁻¹ of cycloheximide (CHX) for 3 min at 37 °C and then washed with PBS containing 100 µg ml⁻¹ CHX. Cells were lysed in polysome extraction buffer (0.5% Triton X-100, 10 mM Tris buffer pH 7.4, 15 mM MgCl₂, 150 mM NaCl, 1 unit µl⁻¹ RNase inhibitor, 100 µg ml⁻¹ CHX); the resulting lysates were layered onto previously prepared linear sucrose density gradients (10–50%). Ultracentrifugation was performed at 35,000 rpm for 2.5 h. Fractions were collected using an ISCO Gradient Former (Model 160; Teledyne ISCO). Total RNA from each fraction was extracted using TRIzol LS reagent (with 2 ng ml⁻¹ in vitro transcribed eGFP mRNA added to monitor RNA extraction efficiency) and reverse transcribed into complementary DNA. qPCR was performed using primers specific for ATR and GAPDH.

³⁵S protein labeling and immunoprecipitation. Cells were treated with DMSO or 40 nM CPT as indicated, cultured in methionine- and cysteine-free DMEM for 30 min at 37 °C before incubation with 250 µCi of ³⁵S methionine and cysteine (EasyTag EXPRESS protein labeling mix [³⁵S], 11 Ci ml⁻¹; PerkinElmer) for an additional 30 min. For pulse-chase studies, labeled cells were returned into normal complete DMEM medium without ³⁵S methionine and cysteine and cultured for the indicated time spans. At the end of the labeling or pulse-chase experiment, the cells were washed with PBS, collected using trypsin and lysed as outlined earlier. The ³⁵S-labeled cell lysates were incubated with ATR (N-19) or GAPDH antibody (Abcam) for 2 h at 4 °C. Antibody-antigen complexes were captured on Dynabeads Protein G (Thermo Fisher Scientific), resolved by 4–12% SDS-PAGE and transferred to PVDF membranes. The membrane was dried and analyzed using the Typhoon storage phosphorimager (GE Healthcare Life Sciences).

Northern blot analysis of tRNAs. TRIzol-purified total RNA was resolved on 10% Tris-borate-EDTA (TBE)-Urea gels, and subsequently transferred for 14 h onto Zeta-Probe nylon membranes (Bio-Rad Laboratories) in 0.5 × TBE at 25 V and 4 °C. After transfer, membranes were cross-linked in a UV Stratalinker 2400 cross-linker (Stratagene), prehybridized with 10 ml ULTRAhyb-Oligo hybridization buffer (Thermo Fisher Scientific) for 1 h at 42 °C and then subjected to hybridization with 10 pmol ³²P-labeled DNA oligo probes (Integrated DNA Technologies) at 42 °C for at least 14 h. Membranes were then rinsed and washed twice with wash buffer (2 × saline sodium citrate with 0.5% SDS) at 42 °C for 1 h, dried and analyzed using the Typhoon storage phosphorimager. The following probe sequences were chosen based on

predictions from the tRNAscan-SE analysis of complete genomes; see URLs^{14,15}:

tRNA Leu-AAG;
AGCCTTAATCCAGCGCTTAGACCGCTGGCCACGCTACC;
tRNA Leu-CAA: GGAGACCAGAACCTTGAGTCTGGCGCCTAGACCA;
tRNA Leu-CAG;
CACGCCTCCAGGGGAGACTGCGACCTGAACGCAGGCCCTT;
tRNA Leu-TAA: CCATTGGATCTTAAGTCCAACGCCCTAACCACTC;
tRNA Leu-TAG: GACTGGAGCCTAACCTCAGGCCCTAGACCC;
tRNA Ser-TGA:
TGGATTTCAGTCCATGCCCTAACCACTCGGCCACGACTAC;
tRNA Ser-AGA;
GATTTCAGTCCATGCCCTAACCACTCGGCCACGACTAC;
tRNA Ser-CGA;
CCCCATTGGATTTCAGTCCAACGCCCTAACCACTCGGCCA;
tRNA Ser-GCT:
GGATTAGCAGTCCATGCCCTAACCACTCGGCCACCTCGTC;
tRNA Thr-TGT: AGGCCCCAGCGAGGATCGAACTCGCGACCCCTGG;
tRNA Val-TAC: TGGTTCCACTGGGGCTCGAACCCAGGACCTTCTGCG;
tRNA Ile-CAT: CCGCTGCGCCACTCTGCT;
5.8S rRNA: TCCTGCAATTACATTAATTCTCGCAGCTAGC.

eGFP expression constructs with synonymous leucine or serine codons. The parental Myc-tagged eGFP pcDNA6.2/gw/d-Topo vector has been described previously¹. eGFP coding sequences in which all leucine or serine residues

are encoded by one distinct codon were synthesized by GenScript and cloned into pcDNA6.2/gw/d-Topo using ApaI and NotI. eGFP protein expression was visualized using anti-GFP immunoblotting, and the corresponding eGFP mRNA levels were determined by qPCR using a primer set targeting the common C-terminal region of all eGFP constructs.

Microscopic imaging. Microscopic imaging of cell cultures was done with a Nikon Eclipse E800 microscope with Nuance FX Multispectral Imaging System (PerkinElmer). The scale bar was generated with ImageJ64 calibration data. Adobe Photoshop was used to minimally adjust the brightness and contrast of entire images. No further digital processing was applied.

Statistical analyses. For all statistical analyses, two-tailed, two-sample equal variance (homoscedastic) Student's *t*-tests were performed using Microsoft Excel. All biological and technical replicates are specified accordingly. Experimental sample sizes were chosen according to commonly accepted ranges for in vitro studies in this field and to achieve statistical significance. For all experiments without statistical analyses, one representative result out of at least three independent experiments is shown.

Reporting Summary. Further information on research design is available in the Nature Research Reporting Summary linked to this article.

Data availability

All data generated and analyzed in this study are available with the paper online.

Life Sciences Reporting Summary

Nature Research wishes to improve the reproducibility of the work that we publish. This form is intended for publication with all accepted life science papers and provides structure for consistency and transparency in reporting. Every life science submission will use this form; some list items might not apply to an individual manuscript, but all fields must be completed for clarity.

For further information on the points included in this form, see [Reporting Life Sciences Research](#). For further information on Nature Research policies, including our [data availability policy](#), see [Authors & Referees](#) and the [Editorial Policy Checklist](#).

► Experimental design

1. Sample size

Describe how sample size was determined.

Experimental sample sizes were chosen according to commonly accepted standards for in vitro studies in this field and to achieve statistical significance.

2. Data exclusions

Describe any data exclusions.

No data were excluded from this study.

3. Replication

Describe whether the experimental findings were reliably reproduced.

At least three independent experiments were performed for each reported data set.

4. Randomization

Describe how samples/organisms/participants were allocated into experimental groups.

No randomization was performed as the study is solely in vitro

5. Blinding

Describe whether the investigators were blinded to group allocation during data collection and/or analysis.

No blinding was required as the study is solely in vitro and does not involve any human/animal subjects.

Note: all studies involving animals and/or human research participants must disclose whether blinding and randomization were used.

6. Statistical parameters

For all figures and tables that use statistical methods, confirm that the following items are present in relevant figure legends (or in the Methods section if additional space is needed).

n/a Confirmed

- The exact sample size (n) for each experimental group/condition, given as a discrete number and unit of measurement (animals, litters, cultures, etc.)
- A description of how samples were collected, noting whether measurements were taken from distinct samples or whether the same sample was measured repeatedly
- A statement indicating how many times each experiment was replicated
- The statistical test(s) used and whether they are one- or two-sided (note: only common tests should be described solely by name; more complex techniques should be described in the Methods section)
- A description of any assumptions or corrections, such as an adjustment for multiple comparisons
- The test results (e.g. *P* values) given as exact values whenever possible and with confidence intervals noted
- A clear description of statistics including central tendency (e.g. median, mean) and variation (e.g. standard deviation, interquartile range)
- Clearly defined error bars

See the web collection on [statistics for biologists](#) for further resources and guidance.

► Software

Policy information about [availability of computer code](#)

7. Software

Describe the software used to analyze the data in this study.

The statistic analyses were done with Microsoft Excel.

For manuscripts utilizing custom algorithms or software that are central to the paper but not yet described in the published literature, software must be made available to editors and reviewers upon request. We strongly encourage code deposition in a community repository (e.g. GitHub). *Nature Methods* [guidance for providing algorithms and software for publication](#) provides further information on this topic.

► Materials and reagents

Policy information about [availability of materials](#)

8. Materials availability

Indicate whether there are restrictions on availability of unique materials or if these materials are only available for distribution by a for-profit company.

All materials used in this study are commercially available.

9. Antibodies

Describe the antibodies used and how they were validated for use in the system under study (i.e. assay and species).

All antibodies used in this study are commercially available from established vendors, validated by its manufacturers, and cited in previous publications.

10. Eukaryotic cell lines

a. State the source of each eukaryotic cell line used.

HEK293, HEK293T: purchased from ATCC®; COLO 357 FG, MIA Paca-2: Dr. Tannishtha Reya at Univ. of California, San Diego.

b. Describe the method of cell line authentication used.

Cell lines were authenticated by ATCC® STR Profiling Services. The STR profile of COLO 357 FG cell line is not a match to any cell line in either the ATCC or the DSMZ STR database. The cell line, (COLO357FG), is not a part of the ATCC collection.

c. Report whether the cell lines were tested for mycoplasma contamination.

All cell lines are tested negative for mycoplasma contamination with MycoAlert™ PLUS Mycoplasma Detection Kit (Lonza).

d. If any of the cell lines used are listed in the database of commonly misidentified cell lines maintained by [ICLAC](#), provide a scientific rationale for their use.

No cell lines used are in the commonly misidentified cell lines list (ICLAC).

► Animals and human research participants

Policy information about [studies involving animals](#); when reporting animal research, follow the [ARRIVE guidelines](#)

11. Description of research animals

Provide details on animals and/or animal-derived materials used in the study.

N/A.

Policy information about [studies involving human research participants](#)

12. Description of human research participants

Describe the covariate-relevant population characteristics of the human research participants.

N/A.